High-resolution measurement of the dielectronic recombination of fluorinelike selenium ions

A. Lampert, A. Wolf, D. Habs, J. Kenntner, G. Kilgus, and D. Schwalm
Max-Planck-Institut für Kernphysik, 69117 Heidelberg, Germany
and Physikalisches Institut der Universität Heidelberg, 69120 Heidelberg, Germany

M. S. Pindzola and N. R. Badnell*
Department of Physics, Auburn University, Auburn, Alabama 36849-5311
(Received 26 July 1995)

We have measured the dielectronic recombination cross section of Se^{25+} ions at center-of-mass energies from 1 to 1800 eV using merged electron and ion beams in the Heidelberg heavy-ion Test Storage Ring (TSR). All dielectronic resonances involving changes of $\Delta N=0$ and $\Delta N=1$ of the core principal quantum number N are covered with high-energy resolution (ranging from <0.6 eV at <90 eV to ≈ 6 eV at 1600 eV). A strong contribution of $\Delta N=1$ Rydberg resonances at 1200–1700 eV is observed. The results are compared with isolated-resonance intermediate-coupling calculations of the cross section. Good agreement is found for the $\Delta N=0$ and the low-lying $\Delta N=1$ resonances. For the $\Delta N=1$ Rydberg series the resonant pattern continues to be well reproduced by theory, whereas the total energy-integrated cross section significantly exceeds the theoretical prediction. From experimental and theoretical results rate coefficients for isotropic plasma temperatures between 100 and 2000 eV are also derived.

PACS number(s): 34.80.Lx

I. INTRODUCTION

Dielectronic recombination (DR) [1,2] has a strong influence on the abundance of ions in different charge states and the population of excited levels in hot, thin plasmas. Recent studies [3] using merged electron and ion beams either in a single-pass arrangement [4] or in an ion storage ring [5–8] as well as measurements using an electron-beam ion trap [9] have provided detailed experimental data about the DR of few electron systems up to boronlike configurations. These measurements were generally in good agreement with theoretical predictions using a ''standard computational method'' [10] in which the total DR cross section is obtained from the radiative and autoionizing decay rates of many individual doubly-excited resonances. For many-electron systems the number of resonances contributing to the DR rate increases strongly. Nevertheless, calculations using this method were performed even for systems with 10 and more electrons [11]. The purpose of the experiment reported here was to test the predictions of the DR cross section for such complex systems using the well-defined experimental conditions and the high energy resolution offered by the merged-beams technique in ion storage rings.

For our study of the DR cross section of a complex highly-charged ion we have chosen the fluorinelike system Se^{25+}, whose recombination with electrons leads into neonlike excited states, some of which are highly relevant for x-ray laser research. In fact, laser gain in the soft-x-ray region was first demonstrated successfully [12] in a laser-produced Se plasma at an electron temperature of about 1 keV, which was composed mainly of Se ions in the fluorine-, neon-, and sodiumlike charge states at about equal fractions. For the $2p^5 3s$-$2p^5 3p$ transition array of the neonlike Se^{24+} ions, plasma-kinetic calculations predict an inversion created mainly by electron-impact excitation from their $2p^6$ ground state [13]. However, also dielectronic recombination is expected to contribute significantly to the population of the relevant Se^{24+} levels [14]. The present measurement of the DR cross section for Se^{25+} appears useful in providing experimental information about the total DR rate coefficient and in testing the reliability of detailed calculations which can be used to derive the partial DR rates into excited Se^{24+} levels. In contrast to a recent measurement of the DR cross section of fluorinelike Xe via the doubly-excited states $2p^4 3l3l'$ in an electron-beam ion trap [15], the present experiment covers the entire energy range of the Rydberg resonances which yield the dominant contribution to the DR rate coefficient at keV electron temperatures. The formation of intermediate doubly excited states involving a change of $\Delta N=1$ of the principal quantum number N of a core electron is described by the capture reactions

$$\mathrm{Se}^{25+}[2s^2(2p^5)_{3/2}]+e^- \rightarrow \begin{cases} \mathrm{Se}^{24+}[2s^2 2p^4\, 3lnl'] & (n=3,\ldots,\infty) \\ \mathrm{Se}^{24+}[2s2p^5\, 3lnl'] & (n=3,\ldots,\infty). \end{cases} \quad (1)$$

The radiative stabilization of these states to singly excited configurations of Se^{24+} (mainly $2s^2 2p^5 nl'$) leads to DR resonances at electron energies between 400 and 1800 eV. At lower electron energies, further contributions to the recombination cross section are caused by radiative recombination and by dielectronic resonances due to capture reactions involving innershell or $\Delta N=0$ excitations according to

*Present address: Department of Physics and Applied Physics, University of Strathclyde, Glasgow G4 0NG, Great Britain.

$$\mathrm{Se}^{25+}[2s^2(2p^5)_{3/2}]+e^- \rightarrow \begin{cases} \mathrm{Se}^{24+}[2s^2(2p^5)_{1/2}nl] & (n=15,\ldots,\infty) \\ \mathrm{Se}^{24+}[2s\ 2p^6nl] & (n=7,\ldots,\infty). \end{cases} \quad (2)$$

To study these processes, we have measured the recombination cross section also at electron energies between ≈ 1 eV and the $2s2p^6$ excitation threshold at ≈ 210 eV. Preliminary results of the present experiment have been presented earlier [16].

II. EXPERIMENT

A. Measurement procedure

The measurements were performed in the heavy-ion Test Storage Ring (TSR) [17] at the Max-Planck-Institut (MPI) für Kernphysik in Heidelberg. Pulses of $^{80}\mathrm{Se}^{25+}$ ions with a kinetic energy of 480 MeV (beam velocity $v_i = 0.113c$) were produced by the MPI tandem and booster facility. Using a stacking technique [18] based on repeated multiturn injection and electron cooling [19] of the stored ion beam, dc currents of up to 100 μA, corresponding to $\approx 3.8\times 10^7$ circulating ions, could be accumulated in the ring. The mean storage time of the ions (210 s at an average residual gas pressure of 5×10^{-11} mbar) was long compared to the decay times of any metastable levels so that the Se^{25+} ions were in their $(2p^5)_{3/2}$ ground state. In one of the straight sections of the storage ring, the circulating ions pass through an electron cooling device and travel inside an intense collinear electron beam over a length of 1.5 m. The electron beam with a diameter of 5.1 cm is confined by a longitudinal magnetic field set to ≈ 50 mT in the present experiment. For electron cooling, which yields typical ion beam diameters of 2–3 mm and a low ion energy spread (see below), the average electron velocity is matched to that of the ions. For recombination measurements, on the other hand, the electron energy in the center-of-mass (c.m.) frame of the ions can be varied over a wide range by changing the electron beam energy while keeping the ion energy fixed. The recombination products are separated from the circulating ion beam at the first dipole magnet downstream of the electron cooling device and counted on a detector. In the present experiment, the recombined Se^{24+} ions were detected by a multichannel plate with a measured efficiency of $>95\%$. After subtraction of the background rate due to electron capture of the Se^{25+} ions in the residual gas and the further data analysis described below, the count rate at this detector yields the recombination cross section, which was measured in this way as a function of the average c.m. electron energy between ≈ 1 and 1800 eV. The corresponding electron energy in the laboratory ranged from ≈ 3.3 keV for matched electron and ion velocities to ≈ 11.5 keV for the highest c.m. energy. The electron density was controlled by the operating conditions of the electron gun and generally increased with the acceleration potential. The count rates for signal and background were of similar magnitude and amounted to $\approx 1\times 10^4\ \mathrm{s}^{-1}$ at values of $\approx 6\times 10^7\ \mathrm{cm}^{-3}$ for the electron density and ≈ 25 μA for the ion current during a typical measurement at higher c.m. energies.

A detailed description of the experimental setup and the measuring technique for DR measurements at the TSR has been given elsewhere [6]. The acceleration voltage of the electron cooling device was set by a high-precision power supply and could in addition be modulated by a square wave at ≈ 12 Hz, adding the output of a high-voltage amplifier with a pulse rise time of ≈ 1 ms and a maximum amplitude of ≈ 1.5 kV. The count rate at the recombination detector was recorded separately for the two levels of the high-voltage modulation. One of the levels was kept *fixed* and usually (except for the scan range of $E<90$ eV discussed below) set in a region where the electron-ion recombination rate was much smaller than the electron capture rate on the residual gas; the rate observed for this level thus provided a continuous measurement of the background. The other level was scanned and the related count rate after subtraction of the count rate at the fixed level provided the energy dependence of the recombination cross section. In this difference signal, the effects of background fluctuations slow compared to the modulation frequency were thus strongly suppressed.

The measuring procedure depended on the scan range of the average c.m. energy E. For $E<90$ eV, the *fixed* level of the modulated acceleration voltage was set to match the electron to the ion velocity, so that quasipermanent cooling, interrupted only for periods short compared to the time constant of the beam heating ($\gtrsim 0.1$ s), could be applied to the ion beam. For a storage lifetime of ≈ 210 s, a nearly constant beam intensity was maintained by injecting ion pulses at intervals of ≈ 10 s, thus replacing the losses. Since electron cooling (typical cooling times $\gtrsim 0.1$ s) remains efficient during the measurement, this scheme strongly suppresses the influence of the ion energy spread on the c.m. energy resolution (see below). Moreover, it avoids variations of the average ion velocity caused by the drag force acting on the ions in the electron beam, as discussed in Ref. [6]. The c.m. energy range where this measuring scheme could be applied was limited by the available modulation amplitude.

For higher energies, the electron beam energy was always detuned from the cooling energy during the energy scans which lasted for ≈ 60 s. Between the scans ions were refilled into the ring while the electron energy was set back to the cooling energy. To compensate the electron drag force, which leads to slow changes of the ion velocity, an induction accelerator was used [6] in the c.m. energy range of 90–210 eV; no such compensation was required in the high energy range of 400–1800 eV. Since no cooling was provided during the measurements in these energy ranges, the ion energy spread increased, in particular by Coulomb collisions within the ion beam (intrabeam scattering). While slow background fluctuations could not affect the difference count rate obtained by the modulation technique described above, slight background variations occurring faster than the modulation period were found to influence the difference signal at the highest electron energies, when the electron beam had the highest intensities and its gas load on the vacuum system became strong enough to cause appreciable pressure variations even within the 12-Hz modulation period. The resulting background in the difference signal corresponded to $<5\%$ of the strongest DR signal in the given energy span and was corrected for by subtracting a linear background from the final cross section, fitted to the noise levels at the scan range limits.

The average ion energy and its spread were monitored [6] during the measurement using the spectrum of the Schottky noise generated by the circulating dc beam, which represents the distribution of the ion revolution frequencies. The contribution of the ions to the c.m. energy spread is given by

$$\Delta E_{\rm ion}=(\Delta E_i/E_i)\sqrt{(m_e/m_i)E_iE}, \tag{3}$$

where E_i is the average ion energy and $\Delta E_i/E_i$ the relative energy spread of the ions in the laboratory frame, while m_e and m_i denote the electron and the ion mass, respectively. The energy spread $\Delta E_i/E_i$ typically amounted to $\approx 2\times 10^{-4}$ during electron cooling; when cooling was stopped the ion beam energy spread and its diameter increased within a few seconds by factors of ≈ 10 and ≈ 2, respectively, but after this initial blow-up the heating rate by intrabeam scattering became much smaller so that $\Delta E_i/E_i$ varied only little during the energy scans with the uncooled ion beam. The electron velocity distribution in the comoving frame is characterized by a transverse temperature $k_BT_\perp=0.1$ eV and a longitudinal temperature of $k_BT_\parallel \lesssim 10^{-3}$ eV. Except for the smallest c.m. energies ($E<10$ eV), the c.m. energy spread is essentially determined by $T_\parallel$ and represented by a full width at half maximum (FWHM) of [6]

$$\Delta E_{\rm el}=4(Ek_BT_\parallel \ln 2)^{1/2}. \tag{4}$$

The effective energy resolution of the DR spectra is given by the total spread $\Delta E=(\Delta E_{\rm ion}^2+\Delta E_{\rm el}^2)^{1/2}$ and varies $\propto E^{1/2}$ as does $\Delta E_{\rm el}$ alone. In the measurements, the total spread ΔE ranged from ≈ 0.6 eV at $E\approx 90$ eV (with quasipermanent ion beam cooling) to ≈ 6 eV at $E=1500$ eV (without ion beam cooling during data taking)—see also Sec. IV.

B. Data analysis

In the standard evaluation procedure of recombination measurements at the TSR described earlier [6], the recombination rate coefficient $\alpha_L(E)$ is obtained from the background-corrected count rate R, the nominal length of the interaction region, $L=1.5$ m, the electron density n_e, the number of stored ions N_i, and the ring circumference $C=55.4$ m using the relation

$$\alpha_L(E)=\frac{R\gamma^2}{Ln_eN_i/C}, \tag{5}$$

where $\gamma^2=[1-(v_i/c)^2]^{-1}\approx 1.006$ is the relativistic transformation factor between the c.m. and the laboratory frame. The quantities N_i and n_e are derived from the ion and electron currents recorded during the scans and from the beam geometry well known for the magnetically guided electron beam. In Eq. (5) the electron density n_e and the average c.m. energy E are assumed to be uniform along the nominal length of the interaction region. The related measured cross section $\sigma_L(E)$ is obtained dividing $\alpha_L(E)$ by the average electron velocity in the c.m. system, which is always large compared to the electron velocity spread in the energy range considered here. The average c.m. energy E is deduced from the ion beam energy and the space-charge corrected electron acceleration potential [6].

For this standard evaluation procedure the principal systematic uncertainty lies in the use of a nominal interaction length L, thereby disregarding the effect of the merging and demerging regions adjacent to the straight interaction zone. Here the electron beam is bent in and out of the ion orbit by toroidal sections of the magnetic guiding field on a radius of 0.8 m for the TSR electron cooler; thus, along their trajectories the ions additionally travel with the electrons for ≈ 0.20 m on either side of the straight interaction zone, where the angle between electron and ion beam—reaching about 14 degrees when the beams separate—and thus the average c.m. energy are increasing. Considering widely spaced narrow resonances in the cross section, the additional contributions to the experimental signal from these merging regions are hardly observable as they spread out over wide energy intervals below the respective resonance energies. Hence, the resonances will still appear as narrow peaks in the measured cross section $\sigma_L(E)$ with widths corresponding to the energy spread ΔE estimated above, and the integrals over such isolated peaks will continue to represent the energy integrated cross sections of the DR resonances in a good approximation. However, the situation changes when densely spaced DR resonances yield a relatively high recombination cross section over an extended c.m. energy range, as in the present experiment. In this case it appears desirable to account in more detail for the merging regions.

To determine the size of the contribution from the merging regions contained in the measured cross section $\sigma_L(E)$, we use our knowledge of the guiding-field geometry from magnetic measurements to calculate the c.m. energy $\tilde{E}(x,E)$ as a function of the position x along the ion beam and of the nominal c.m. energy E. This calculation includes variations of the angle between the electron and ion beams also within the nominal interaction zone, in particular in the transition region between the solenoidal and the toroidal sections of the magnetic guiding field. The rate coefficient for an ideal situation without merging regions, denoted by $\alpha(E)$, is then given by

$$\alpha(E)=\alpha_L(E)-\Delta\alpha(E), \tag{6}$$

where the correction $\Delta\alpha(E)$ amounts to

$$\Delta\alpha(E)=L^{-1}\int \alpha(\tilde{E}(x,E))dx-\alpha(E). \tag{7}$$

Here, the integral extends over the complete overlap length of the electron and ion beams. For the energy-averaged experimental cross section, found from the rate coefficient α by dividing it by the average c.m. velocity, the corresponding relations are

$$\sigma(E)=\sigma_L(E)-\Delta\sigma(E), \tag{8}$$

where the correction $\Delta\sigma(E)$ amounts to

$$\Delta\sigma(E)=L^{-1}\int \sqrt{\frac{\tilde{E}(x,E)}{E}}\sigma(\tilde{E}(x,E))dx-\sigma(E). \tag{9}$$

Formally, Eqs. (8) and (9) represent an integral equation which can be solved iteratively in order to find $\sigma(E)$ for $\sigma_L(E)$ and $\tilde{E}(x,E)$ given. The correction $\Delta\sigma(E)$ can be

found by initially setting $\sigma(E)=\sigma_L(E)$ in Eq. (9) and using the resulting $\Delta\sigma(E)$ in the right-hand side of Eq. (8) to determine a new estimate of $\sigma(E)$, for which the procedure is repeated. Results for $\Delta\sigma(E)$ with numerical accuracies well below 1% were obtained after usually <15 iterations. We note that in this experiment the energy $\tilde{E}(x,E)$ deviated from the nominal average c.m. energy E due to the angle between electrons and ions in the merging regions by up to 180 eV at $E=0$ and by up to 325 eV at $E=2000$ eV.

This correction was applied to all data presented. The systematic error of the absolute cross-section scale is estimated to be $\pm 15\%$, where the dominant error stems from the particle current measurement and the detector efficiency. The influence of the inaccurate knowledge of the effective overlap length L, which contributes to the systematic error of the cross section scale when using the standard evaluation procedure [6], is strongly reduced by the merging-region correction. The relative uncertainty in comparing values of the cross section measured at largely different energies is estimated to be $\pm 5\%$. The error of the absolute energy scale is estimated to be ± 0.4 eV and ± 1.8 eV for c.m. energies of 80 and 1000 eV, respectively, and roughly scales as $\propto E^{1/2}$; an additional uncertainty of about ± 0.3 eV is expected in the energy range between 90 and ≈ 150 eV, where the drag force of the electron cooler is relatively strong and could be compensated only approximately by the induction accelerator mentioned above.

III. THEORY

A calculation of the DR cross section caused by the resonances described by Eqs. (1) and (2) was performed in the isolated-resonance approximation, finding the energy-integrated cross section $\hat{\sigma}_d$ due to a doubly-excited resonance d from its autoionization and radiative decay rates A_a, A_r according to the relation

$$\hat{\sigma}_d=\frac{2\pi^2}{k^2}\,\frac{g_d}{2g_i}\,\frac{A_a(d\to i)\Sigma_f A_r(d\to f)}{\Sigma_\kappa A_a(d\to\kappa)+\Sigma_{f'}A_r(d\to f')}. \qquad (10)$$

Here, g_d and g_i denote the statistical weights of the resonance and the initial $(2p^5)_{3/2}$ core, respectively, k is the linear momentum of the incident electron, and atomic units are used. The energies and decay rates were obtained using the AUTOSTRUCTURE package [20]. The summation variable f in Eq. (10) symbolizes the bound configurations of Se^{24+}, i.e., $(2p^5)_{3/2}nl$, $(2p^5)_{1/2}nl$ $(n<15)$, and $2s2p^6nl$ $(n<7)$. The summation variables f' and κ denote all decay channels contributing to the total autoionization and radiative decay widths of the resonance. Rydberg resonances were included up to a maximum quantum number n corresponding to the estimated experimental cutoff [6] for detecting Se^{24+} ions formed in highly excited states.

The theoretical results for $\hat{\sigma}_d$ are combined into an energy-averaged DR cross section

$$\bar{\sigma}(E)=(1/\delta E)\sum_d^{(E,\delta E)}\hat{\sigma}_d, \qquad (11)$$

where the sum at a given energy E runs over all resonances in an energy bin $(E,\delta E)$ of width δE centered at E. The width δE is chosen to be large compared to the decay width of the resonances and small compared to the experimental resolution; it varied between 0.1 eV for the energy range 0–80 eV and 0.6 eV for the range 1200–1800 eV. For a comparison with the measured cross section, the result of Eq. (11) is then convoluted with the experimental c.m. energy distribution; at c.m. energies $E\gtrsim 10$ eV we use a Gaussian with a width ΔE accounting for the longitudinal ion and electron velocity spread, as discussed in Sec. II.A., and at lower energies both the transverse and the longitudinal velocity spread of the electrons are taken into account by using an appropriate asymmetric energy distribution [6].

Two types of intermediate-coupling atomic-structure calculations were carried out to obtain the resonance energies, autoionization decay rates, and radiative decay rates needed for the evaluation of Eq. (10). The first method, which we call perturbative-relativistic, solves standard radial Schrödinger equations for all bound and continuum orbitals and then diagonalizes a Hamiltonian which includes the kinetic energy, the electrostatic potential energy, and one-body relativistic terms to obtain resonance energies and wave functions. First-order many-body perturbation theory is then applied to obtain autoionization and radiative rates using the previously calculated energies and wave functions. The second method, which we call semirelativistic, uses the radial Schrödinger equations including the relativistic kinetic energy correction and Darwin terms and a Hamiltonian with the kinetic energy, electrostatic potential energy, and spin-orbit terms. The computer code AUTOSTRUCTURE calculates cross sections for low n explicitly and for high n by extrapolating radial wave functions using quantum-defect theory. In general, configuration interaction within a complex is included for low n, while high-n $(n\geqslant 5)$ contributions are calculated in a single-configuration approximation. For relatively low-charged ions, like Se^{25+}, we ignore Breit interaction and QED corrections, and multipolar terms beyond $E1$ in the calculation of the radiative decay rates.

IV. RESULTS AND DISCUSSION

A. $\Delta N=0$ DR

In Fig. 1(a) we show an overview of the measured recombination cross section of Se^{25+} ions with low-energy electrons, covering the range of intrashell DR resonances according to Eq. (2). The low-energy resonances can be attributed to the $(2p^5)_{1/2}$ excitation which leads to a Rydberg series with a limit at ≈ 43 eV. The amplitudes of the higher Rydberg resonances of this series decrease rapidly so that no structure occurs in the measured spectrum at the series limit. A second series of resonances can be attributed to the excited core state $2s2p^6$ and leads to a Rydberg peak with a cross section of $\approx 1.3\times 10^{-19}$ cm^2 at the series limit (≈ 210 eV). For the lower members of this series, the fine structure is partly resolved. In the low-energy region, also a contribution due to nonresonant radiative recombination is clearly visible in the observed cross section; it will be discussed in more detail in Sec. IV.B.. As explained in Sec. II.A., the spectra above and below 90 eV were obtained using different measuring procedures. The spectra in the low energy range offer a better energy resolution than those for the higher energy range. On the other hand, in these spectra the background

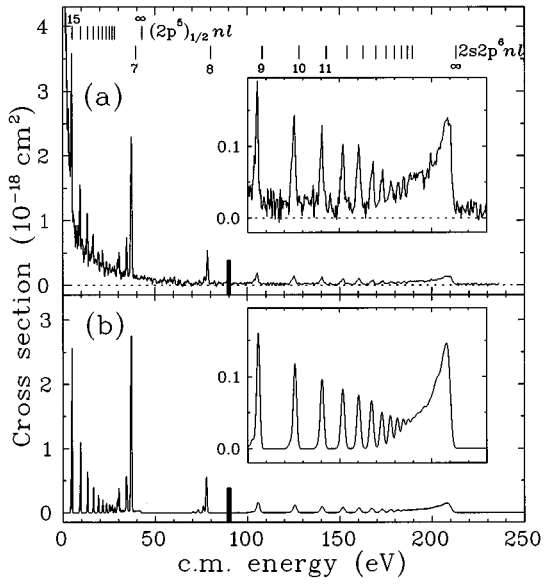

FIG. 1. (a) Measured free-electron capture cross section $\sigma(E)$ and (b) calculated DR cross section for Se^{25+} ions as a function of the average c.m. electron energy E showing two Rydberg series of $\Delta N=0$ DR resonances [Rydberg energies $E_\infty-(25/n)^2\mathscr{R}$ indicated by vertical bars]. The measured cross section includes the signal due to nonresonant radiative recombination, which decreases with increasing energy. The mark at 90 eV indicates the border line between the two energy ranges where different measuring procedures have been used. The theory shows only the resonant contribution to the cross section, convoluted with the experimental c.m. energy distributions as specified in the text.

due to electron capture of Se^{25+} ions in the residual gas has to be removed separately; this was done by subtracting a *constant* such that the signal count rate at 89 eV agreed with the one expected from radiative recombination (cf. Sec. IVB). In the higher energy range the background due to electron capture in the residual gas was continuously measured and subtracted using the modulation technique described in Sec. IIA, but since the count rate at the fixed reference level still contained a finite contribution from radiative recombination, a constant level was added to the difference count rate so that again the resulting signal rate agreed with that expected for radiative recombination at 89 eV.

Figure 1(b) shows the calculated DR cross section, folded with the experimental c.m. energy distribution as discussed in Sec. III, including Rydberg resonances with $n\leqslant 100$. The energy distribution used below 90 eV, where the cross section was measured with a quasipermanently cooled ion beam (see Sec. IIA), accounts for the electron temperature only. The transverse temperature was set to $kT_\perp=0.1$ eV corresponding to the cathode temperature [6]. The longitudinal temperature was determined from the observed FWHM of the $2s2p^6\,8l$ resonances at 78 eV. By a Gaussian fit to the cross section, taking into account the fine structure splitting, a total c.m. energy spread of $\Delta E=0.6$ eV is obtained. Neglecting the influence of the ion energy spread on the total spread we set $\Delta E_{\rm el}=\Delta E$, which yields a longitudinal electron temperature of $kT_\parallel=0.42\times10^{-3}$ eV using Eq. (4).

Above 90 eV, where the ion beam could not be cooled during the measurements, the c.m. energy spread increases because of the ion energy spread according to Eq. (3). This effect was studied in detail measuring the $2s2p^6\,8l$ resonances at 78 eV also with the procedure normally used only above 90 eV. An energy spread of $\Delta E=1.4$ eV was observed as compared to the value of $\Delta E=\Delta E_{\rm el}=0.6$ eV observed before. Simultaneously, an ion energy spread of $\Delta E_i/E_i=2.4\times10^{-3}$ was deduced from the Schottky spectrum. Combining the corresponding energy spread $\Delta E_{\rm ion}$ from Eq. (3) at the given resonance energy with the electron contribution $\Delta E_{\rm el}$ determined above, we obtain $\Delta E=(\Delta E_{\rm ion}^2+\Delta E_{\rm el}^2)^{1/2}=1.4$ eV, in agreement with the observed energy spread. Hence, the theoretical cross section above 90 eV in Fig. 1 is folded with a Gaussian c.m. energy distribution whose width corresponds to this ΔE scaled $\propto E^{1/2}$ according to the discussion in Sec. IIA.

TABLE I. Measured and calculated resonance energies E_n and energy-integrated, l-summed DR cross sections $\hat\sigma_n$ of Se^{25+} ions for the $(2p^5)_{1/2}nl$ doubly excited states.

	E_n (eV)		$\hat\sigma_n$ (10^{-21} cm^2 eV)	
n	Expt. [a]	Theory	Expt. [a]	Theory
15	4.93 ± 0.01	4.96	972.4 ± 123	997
16	9.47 ± 0.01	9.49	433.6 ± 92	417
17	13.24 ± 0.02	13.36	285.9 ± 41	245
18	16.47 ± 0.03	16.57	171.1 ± 40	164
19	19.22 ± 0.06	19.29	120.6 ± 50	119
20	21.48 ± 0.06	21.56	96.9 ± 17	91
>20			<500	486

[a]Statistical errors only.

Very good overall agreement is found (see Fig. 1) between the folded theoretical DR spectrum and the resonant contributions to the experimental cross section. The resonance energies E_n and integrated cross sections $\hat\sigma_n$ for individual DR peaks were determined from the measured cross section $\sigma(E)$ by fitting the theoretical line shape function [6] plus a smooth background describing the nonresonant contribution. For the Rydberg series $(2p^5)_{1/2}nl$, a detailed comparison between the experimental and theoretical results is presented in Table I. The resonances of this series are associated with a core excitation in which only the angular momentum coupling within the $2p^5$ shell is changed. An electron captured in one of the doubly excited states $(2p^5)_{1/2}nl$ can stabilize radiatively mainly by a transition of the Rydberg electron to a nonautoionizing $(2p^5)_{1/2}nl$ state of Se^{24+} with $n<15$, while the spontaneous radiative decay of the $(2p^5)_{1/2}$ core state back to the $(2p^5)_{3/2}$ ground state is too slow (decay rate 0.4 μs^{-1}). Taking the simple scaling laws [21] of $A_a=c_a n^{-3}$ and $A_r=c_r n^{-3}$, one expects the integrated DR cross sections $\hat\sigma_n$ of the Rydberg resonances to vary as

$$\hat\sigma_n\propto E_n^{-1}n^{-3}c_a/(1+c_a/c_r). \tag{12}$$

This implies a rapid decrease of the DR cross section with increasing n and very small contributions of high-lying Rydberg states close to the series limit, which is an unsual situation for the DR via $\Delta N=0$ resonances. The measured cross section of the $(2p^5)_{1/2}nl$ doubly excited states, multiplied by the resonance energy E_n to eliminate the variation

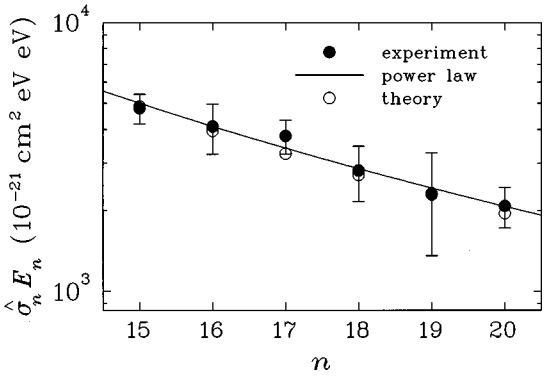

FIG. 2. Measured and calculated DR resonance strength $\hat{\sigma}_n E_n$ as a function of the principal quantum number n for the series $(2p^5)_{1/2}nl$. The curve represents the power law $\hat{\sigma}_n E_n = an^b$ with fitted constants a and b (see text).

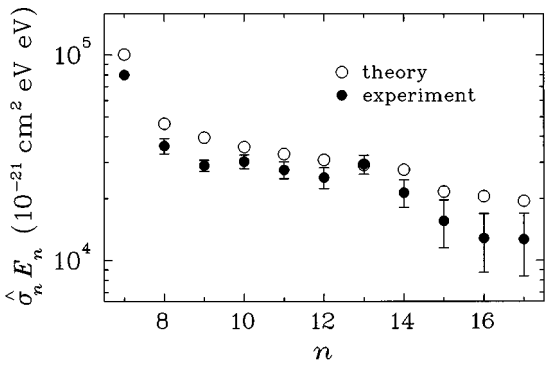

FIG. 3. Measured and calculated DR resonance strength $\hat{\sigma}_n E_n$ as a function of the principal quantum number n for the series $2s2p^6nl$.

$\hat{\sigma}_n \propto E_n^{-1}$, is shown as a function of n in Fig. 2. Fitting a power law to the measured cross section yields an exponent of -3.0 ± 0.4 in accordance with Eq. (12).

The theoretical values of the cross section and the resonance energy, listed in Table I, are in good agreement with the experimental results. A fit of the Rydberg formula $E_n = E_\infty - \mathscr{R}(25/n)^2$, where $\mathscr{R}$ denotes the Rydberg energy constant, yields a series limit of $E_\infty = 42.70 \pm 0.01$ eV. This value has to be compared with a more precise experimental result of 42.91 eV from Ref. [22]. The small deviation of ≈ 0.2 eV is consistent with the estimated systematic error of the absolute energy scale (± 0.3 eV).

For the second series of $\Delta N = 0$ resonances, $2s2p^6nl$, experimental and theoretical results are listed in Table II. The energies and individual cross sections of the resolved fine structure terms for $n = 7,8$ are discussed below. As for the other innershell DR series, the limit E_∞ can be obtained from a fit of the Rydberg formula to the observed resonance energies. The result, representing the excitation energy $2s^2(2p^5)_{3/2}$-$2s2p^6$, is $E_\infty = 210.74 \pm 0.1$ eV and agrees well with the value of 210.80 eV from Ref. [22]. To explain the n dependence of the resonance strength (see Fig. 3), a somewhat more complicated model than for Fig. 2 is needed, which reflects the different possibilities of radiative stabilization as well as the opening of new autoionization channels. Thus, the drop of $\hat{\sigma}_n E_n$ between $n = 7$ and $n = 8$ is caused by the opening of the additional autoionization channel $2s2p^6nl \rightarrow 2s^2(2p^5)_{1/2} + e$ near 43 eV (cf. Fig. 1). For higher n, the resonance strength $\hat{\sigma}_n E_n$ first tends to a constant value, which indicates that the dominant stabilization processes leading to DR occur with the Rydberg electron as a spectator and are represented by radiative transitions within the core, forming the states $2s^2(2p^5)_{3/2}nl$ and $2s^2(2p^5)_{1/2}nl$. As usual for $\Delta N = 0$ DR, the decrease of the autoionization rate described by $A_a = c_a n^{-3}$ affects the cross section [see Eq. (10)] only for very high Rydberg levels close to the series limit. On the other hand, since the Rydberg states $2s^2(2p^5)_{1/2}nl$ are stable against autoionization only for $n < 15$, a second drop of the resonance strength occurs at $n = 15$, and the size of this decrease indicates the relative importance of the radiative core transition $2s2p^6$-$2s^2(2p^5)_{1/2}$.

TABLE II. Measured and calculated resonance energies E_n and energy-integrated, l-summed DR cross sections $\hat{\sigma}_n$ of Se^{25+} ions for the $2s2p^6nl$ doubly excited states.

	E_n (eV)		$\hat{\sigma}_n$ (10^{-21} cm^2 eV)	
n	Expt. [a]	Theory	Expt. [a]	Theory
7			2226 ± 60	2678
8			462 ± 40	601
9	105.0 ± 0.1 [b]	105.65	276 ± 17	376
10	125.2 ± 0.1 [b]	125.56	242 ± 18	284
11	140.3 ± 0.1 [b]	140.05	197 ± 18	235
12	151.7 ± 0.1 [b]	151.77	167 ± 19	204
13	160.4 ± 0.1	160.42	183 ± 20	182
14	167.7 ± 0.2	167.24	128 ± 20	165
15	173.2 ± 0.3	172.74	90 ± 24	125
16	178.0 ± 0.4	177.46	72 ± 23	116
17	181.8 ± 0.4	181.39	68 ± 24	107
>17			1732 ± 150	2010

[a] Statistical errors only.

[b] Additional uncertainty of ± 0.3 eV for these energies by possible shifts of the ion energy (see text).

It is seen from Table II and Fig. 3 that the theory describes the measured n dependence of the cross section but overestimates its absolute value by approximately 20%. More specific information about the origin of this discrepancy can be obtained by considering the individual cross sections $\hat{\sigma}_{nl}$ of the resolved fine structure terms for $n = 7,8$ listed in Table III. The calculated cross sections for $l \leqslant 2$ agree reasonably with the measured values, whereas the total contribution of the unresolved resonances with higher l is clearly overestimated. This is also evident from the direct comparison of the measured and the calculated cross section near the $2s2p^67l$ resonances in Fig. 4. Because of the high statistical weight of the high-l states, predictions of the DR cross section are particularly sensitive to the l dependence of the autoionization rate, which decreases for higher orbital angular momentum.

B. Radiative recombination

Nonresonant radiative recombination (RR) occurs preferably at low c.m. energies E. For energies $E \ll q^2 \mathscr{R}$ the cross

TABLE III. Measured and calculated resonance energies E_{nl} and energy-integrated DR cross sections $\hat{\sigma}_{nl}$ of Se^{25+} ions for the resolved sublevels of the doubly excited states $2s2p^6nl$, $n=7,8$.

	E_{nl} (eV)		$\hat{\sigma}_{nl}(10^{-21}$ cm^2 eV)	
nl	Expt. [a]	Theory	Expt. [a]	Theory
$7s$		26.0	<20	51
$7p_{1/2}$	29.63 ± 0.05	29.76	108 ± 23	123
$7p_{3/2}$	30.47 ± 0.03	30.57	197 ± 20	176
$7d$	34.51 ± 0.01 [b]	34.4	339 ± 31	402
$7l$ ($l>2$)	37.23 ± 0.01 [b]	37.1	1582 ± 39	1926
$n=7$ (sum)			2226 ± 60	2678
$8s$		70.6	<20	10
$8p$		73.1	<20	43
$8d$	76.6 ± 0.1 [b]	76.0	79 ± 21	84
$8l$ ($l>2$)	78.4 ± 0.1 [b]	77.8	383 ± 20	463
$n=8$ (sum)			462 ± 40	601

[a]Statistical errors only.
[b]Energy of dominant peak.

section varies roughly as $\propto E^{-1}$ and final Rydberg levels give a large contribution to the total RR rate. A theoretical prediction can be obtained from the semiclassical hydrogenic RR cross section given by Kramers [23] and by Bethe and Salpeter [24]. RR cross sections for multicharged ions measured in earlier merged-beams experiments [25–28] could (except for significant deviations at very low energies $\lesssim 0.01$ eV found in some experiments [26–28], see below) be well reproduced by this description introducing a suitable effective nuclear charge $Z_{\rm eff}$ for ions with a few-electron core. For a $2s^2(2p^5)_{3/2}$ core the total cross section assumes the form

$$\sigma^r(E)=\sum_{n=3}^{n_{\rm cut}}\sigma_n^r(E)+\tfrac{1}{32}\sigma_2^r(E) \qquad (13)$$

with [24]

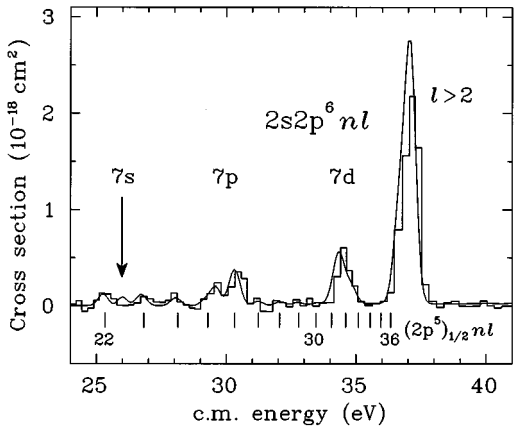

FIG. 4. DR cross section at energies around the $2s2p^6\,7l$ resonances. The measured data after subtraction of a smooth fitted function representing the nonresonant background are shown by a histogram. The theoretical cross section (smooth curve) was folded with the experimental c.m. energy distribution. The weak $(2p^5)_{1/2}nl$ Rydberg resonances, converging to a series limit at ≈ 43 eV, are marked below the curves.

$$\sigma_n^r(E)=\frac{32}{3\sqrt{3}}\alpha^3\pi a_0^2\frac{Z_{\rm eff}^4\mathscr{R}^2}{n(Z_{\rm eff}^2\mathscr{R}+n^2E)}, \qquad (14)$$

where α is the fine structure constant and a_0 the Bohr radius. The almost filled $n=2$ shell yields only a small contribution to the total RR cross section in Eq. (13). In comparison to the contribution $\sigma_2^r(E)$ of a completely open $n=2$ shell (where the statistical weight of the core and the final state amount to 1 and 8, respectively) the cross section for the transition $(2p^5)_{3/2}+e\rightarrow 2p^6$ with the same $Z_{\rm eff}$ is reduced by a factor of $g_f/8g_i=1/32$ according to the statistical weights of $g_i=4$ for the $(2p^5)_{3/2}$ core and $g_f=1$ for the $2p^6$ final state. The upper limit $n_{\rm cut}$ of the sum in Eq. (13) represents the highest quantum number for which the ions formed by RR can reach the recombination detector. This limit is caused by the field ionization of recombined ions in highly excited states when they pass through the storage ring magnets between the interaction region and the detector, as discussed in more detail in Ref. [6]. For the present measurement, we estimate $n_{\rm cut}=150$.

As can be seen from Eq. (14), the cross section for a final state with a principal quantum number $n\ll n_{\rm max}(E)=(Z_{\rm eff}^2\mathscr{R}/E)^{1/2}$ decreases rather slowly ($\propto n^{-1}$) as n increases; for $n\gg n_{\rm max}(E)$, however, the n dependence of the cross section changes to $\sigma_n^r(E)\propto n^{-3}$. Thus, at a given electron energy E the dominant contribution to the RR cross section comes from states with $n\leqslant n_{\rm max}(E)$. The value of $n_{\rm max}$ varies from 92 at 1 eV to 10 at 90 eV. Since the estimated experimental cutoff $n_{\rm cut}=150$ is considerably higher than $n_{\rm max}$, it is expected to have a very small influence on the total cross section $\sigma^r(E)$ for $E\gtrsim 1$ eV. On the other hand, the high values of $n_{\rm max}$ suggest that the hydrogenic approximation with a choice of $Z_{\rm eff}=q=25$ for the effective nuclear charge should be adequate. This is also supported by a distorted-wave calculation of the RR cross section in which we summed the partial cross sections up to $n_{\rm cut}$; this result was found to coincide within 10% with the hydrogenic cross section from Eqs. (13) and (14) for $Z_{\rm eff}=q=25$ over the energy range from 1 to 100 eV.

The experimental rate coefficient at lower c.m. energies is plotted in Fig. 5 together with the theoretical RR rate coefficient calculated from Eqs. (13) and (14) setting $Z_{\rm eff}=25$.[We here show the rate coefficients $\alpha(E)$ defined by $(2E/m)^{1/2}\sigma(E)$ instead of $\sigma(E)$ since they vary less strongly with the energy.] With the measured signal adjusted to the theoretical RR rate at 89 eV (see Sec. IVA), the experimental rate coefficient confirms the trend of the theory over the adjacent energy range up to 230 eV and down to 50 eV. At lower energies between 50 eV and ≈ 10 eV the theory fails to reproduce the experimental signal, which is observed to be considerably higher than predicted. The reason of this discrepancy is not well understood; since it appears in the low scan range where no simultaneous measurement of the background count rate was available (see Sec. IIA) it cannot be excluded that variations of the residual-gas pressure during the scan have caused a systematic dependence of the background rate on the c.m. energy. Apart from this, a reasonable description of the observed nonresonant recombination signal between ≈ 1 and 230 eV is obtained using the theoretical

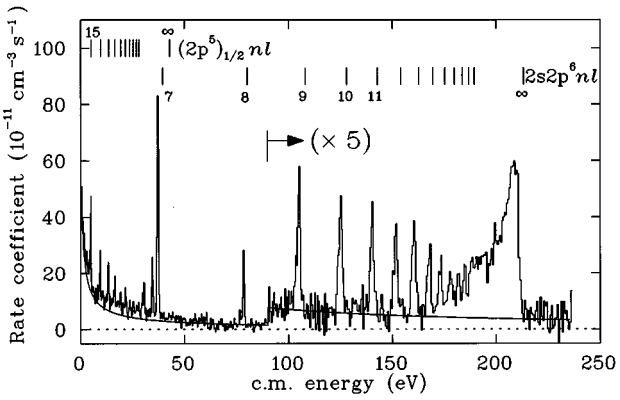

FIG. 5. Measured recombination rate coefficient $(2E/m_e)^{1/2}\sigma(E)$ for low energies, showing the nonresonant radiative recombination signal and the DR resonances of the $(2p^5)_{1/2}$ and $2s2p^6$ series as indicated by the vertical bars. Also plotted is the RR rate coefficient calculated from Eqs. (13) and (14) using $Z_{\text{eff}}=q=25$. The experimental cross section was matched to the theoretical RR cross section at 89 eV as described in the text.

RR cross section from the hydrogenic model of Eqs. (13) and (14).

The spontaneous recombination rate during electron cooling (fixed electron energy corresponding to $E=0$) was measured to be $(4.8\pm0.4)\times10^{-9}$ cm^3 s^{-1}; compared to the RR rate coefficient calculated from Eqs. (13) and (14) for the given electron temperatures, this indicates an enhancement by a factor of 2. The enhancement observed here seems to be of the same nature as the one seen with other multicharged ions under equivalent conditions at the TSR [6,26,28] and in one experiment with single-pass merged electron and ion beams [27]. As discussed earlier [28], the results and the experimental parameters of different measurements indicate that the rate enhancement may be related to the low electron velocity spread in longitudinal direction (corresponding to a thermal energy of <1 meV) and to the presence of a longitudinal magnetic guiding field for the electron beam. Possible explanations of this phenomenon are presently under discussion [29], and recent experimental results [30] clearly indicate that the enhancement occurs in a limited range of electron energies ($E\lesssim0.01$ eV); hence it should not have an impact on the DR measurements of the present work.

C. $\Delta N=1$ DR

The dielectronic resonances corresponding to the reactions listed in Eq. (1) are distributed over the energy range of 400–1800 eV. These c.m. energies were covered by five overlapping scans each ≈400–600 eV wide. As described in Sec. IIA, the background due to electron capture of Se^{25+} ions in the residual gas was continuously measured and subtracted using the count rate at a fixed energy within each of the scan ranges, where no DR signal was present and the RR signal could be neglected owing to the high c.m. energy. The results in the overlap regions of the energy scans were found to agree within the statistical errors and thus were averaged. An overview of the measured cross section is given in Fig. 6(a).

From the tabulated excitation energies [22] of Se^{25+}, one can identify the dominant Rydberg series of DR resonances,

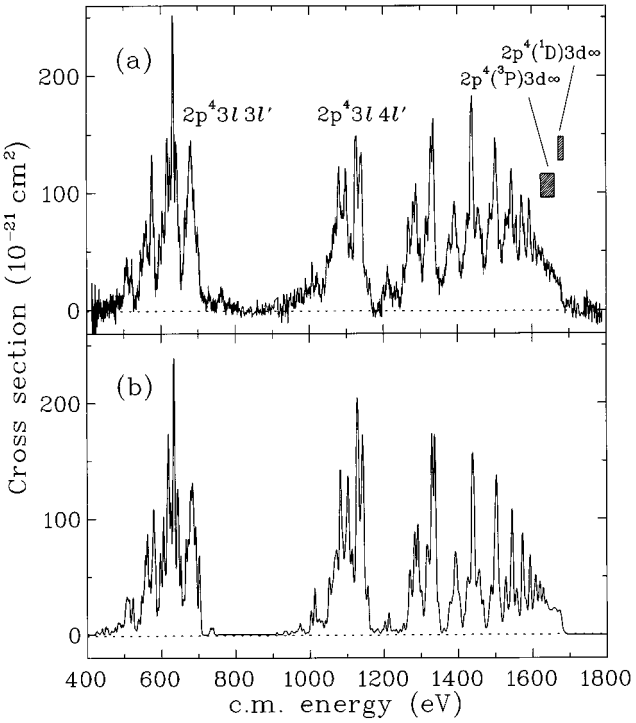

FIG. 6. (a) Measured free-electron capture cross section $\sigma(E)$ and (b) calculated DR cross section of Se^{25+} ions via the $\Delta N=1$ resonances. The dominant peaks are due to the $2p^4\,3lnl'$ doubly excited states. The energy ranges of the various excitation thresholds $2p^4(^1D)3d\infty$ and $2p^4(^3P)3d\infty$ are indicated by the shaded regions. The theory was convoluted with the experimental c.m. energy distribution discussed in the text and includes Rydberg resonances with principal quantum numbers $n\leqslant100$.

corresponding to the excitations $2p^4(^1D)3d$ (1671–1686 eV) and $2p^4(^3P)3d$ (1624–1662 eV), which give rise to several series limits in the given energy regions. Significant contributions to the DR cross section are not observed near the excitation thresholds $2p^4(^1S)3d$ (≈1723 eV) and $2s2p^5(^1P)3p$ (1737–1823 eV). The structure due to the $2p^4 3s$ excitation thresholds (≈1500–1600 eV) cannot be identified among the strong peaks in this energy region, which obviously belong to the dominant $2p^4 3d$ series. At lower energies, the $3l3l'$ resonances are clearly separated. The $3l4l'$ and $3l5l'$ resonances can still be identified as separate manifolds extending over ≈280 eV and ≈180 eV, respectively, whereas the higher manifolds $3lnl'$ ($n\geqslant6$) are already overlapping. The large integrated cross section resulting from the Rydberg manifolds leads to a relatively strong influence of the merging regions of the electron and ion beams on the experimental cross section. To indicate the size of this contribution, the correction $\Delta\sigma(E)$ determined according to Sec. IIB and the uncorrected cross section $\sigma_L(E)$ are plotted in Fig. 7. It is seen that, because of the merging regions, the peaks of the different manifolds are accompanied by broad low-energy tails which, in the uncorrected cross section, sometimes add significantly to the cross section observed at lower manifolds and to the background level. The correction for merging-region effects is thus important for avoiding artefacts, in particular in the energy-integrated cross section discussed below. More narrow struc-

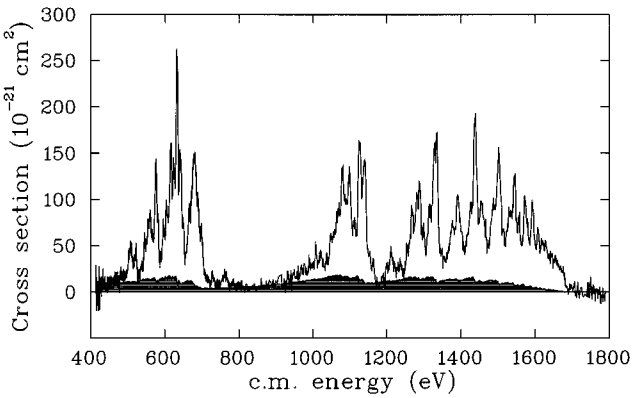

FIG. 7. Measured cross section $\sigma_L(E)$ for the $\Delta N=1$ resonances, as deduced using the standard evaluation procedure, and the correction $\Delta\sigma(E)$ (shaded area) which accounts for the merging regions of the electron and the ion beams and which was subtracted from $\sigma_L(E)$ to obtain the experimental cross section $\sigma(E)$.

tures in the correction $\Delta\sigma$ occurring at sharp resonances in the cross section reflect the peak broadening caused by variations of the angle between the electron and the ion beam over a fraction of the nominal interaction zone, which are also included in the function $\tilde{E}(x,E)$ (see Sec. IIB).

The theoretical DR cross section, shown in Fig. 6(b), was obtained as discussed in Sec. III and folded with a Gaussian energy distribution. The experimental energy spread ΔE was scaled up according to the expected energy dependence $\propto E^{1/2}$ from the value of $\Delta E=1.4$ eV observed for an uncooled ion beam at $E=78$ eV (see Sec. IVA). This yields $\Delta E\approx 4$ eV at 600 eV and $\Delta E\approx 6$ eV at 1600 eV. The resonant structures observed in the experiment are well reproduced by the folded theoretical spectrum. The quantitative agreement is particularly good for the $3l3l'$ resonances, depicted in detail in Fig. 8. The use of relativistic wave functions is important to reproduce the energy positions and the resonance strengths, especially in the range of 500–600 eV,

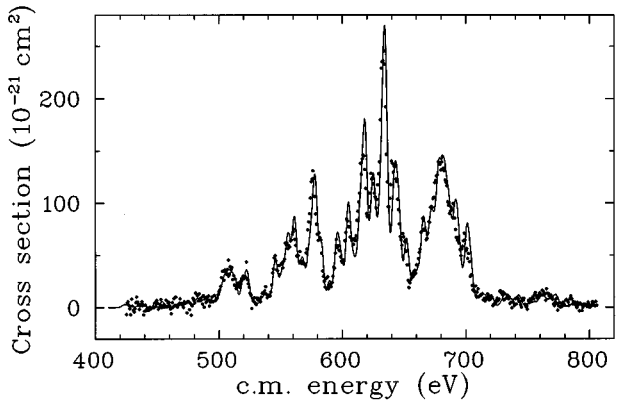

FIG. 8. Measured free-electron capture cross section $\sigma(E)$ (dots) and calculated DR cross section (smooth curve) due to the $2p^4\,3l3l'$ and $2s2p^5\,3l3l'$ doubly excited states. The theory was convoluted with a Gaussian of 4 eV FWHM, representing the experimental c.m. energy distribution. Weak $2s2p^5\,3l3l'$ resonances can be seen at energies $\gtrsim 710$ eV.

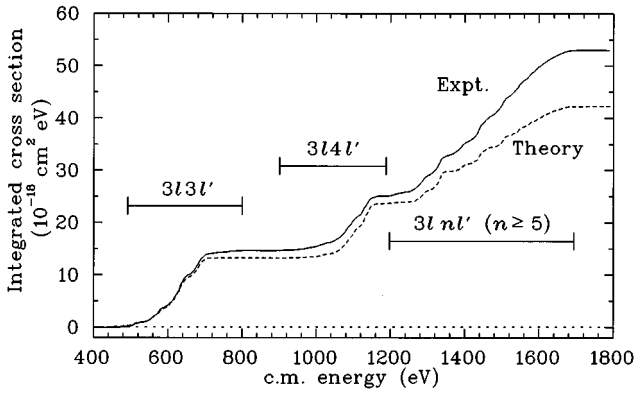

FIG. 9. Energy-integrated cross section of the $\Delta N=1$ DR resonances, shown as a function of the upper limit of the integration range (lower limit 400 eV) for experiment (full line) and theory (broken line).

as shown by calculations where nonrelativistic Thomas-Fermi wave functions were used. The calculation for this resonance group also shows that the dominant resonances are due to the $2p^4$ core excitation, whereas the contribution of the resonances with a $2s2p^5$ core is less than 10% of the total $3l3l'$ cross section.

Because of the large number of doubly-excited states giving rise to DR resonances which are not resolved at the present c.m. energy spread, we cannot give a state-by-state comparison of experimental and theoretical results. However, in Fig. 9 we present a comparison of the energy-integrated experimental and theoretical cross sections for the $\Delta N=1$ DR resonances between 400 eV and a variable upper limit of integration. For the integrated cross sections of the $3l3l'$ and $3l4l'$ manifolds, the theoretical integrated cross section differs from the experimental one by less than 10%, whereas the difference increases up to $\approx 20\%$ when the integral includes also the higher-n manifolds. Thus, the relative contribution of the high-n states is underestimated by more than the systematic error of the experiment ($\pm 5\%$ for relative contributions). The discrepancy might be explained by the fact that in contrast to the $n\leqslant 4$ manifolds the high-n ($n\geqslant 5$) contributions are calculated in a single-configuration approximation only. Many weak DR resonances underestimated by the theory may add up to yield an additional contribution to the measured cross section with a rather smooth energy dependence because of the finite energy resolution. Some weaker, apparently underestimated resonances can be seen in Fig. 6(b), in particular on the low-energy side of the manifold $3l5l'$ (1180–1260 eV).

D. Rate coefficients for high-temperature plasmas

From the measured and calculated recombination cross sections we can derive total DR rate coefficients for Se^{25+} ions in a plasma with a Maxwellian electron energy distribution at a given temperature T_e by

$$\alpha(T_e)=\frac{4}{(2\pi m_e k_B T_e)^{1/2}}\int_0^\infty \frac{E}{k_B T_e}e^{-E/k_B T_e}\sigma(E)dE. \tag{15}$$

The resulting rate coefficients via the $\Delta N=0$ and the

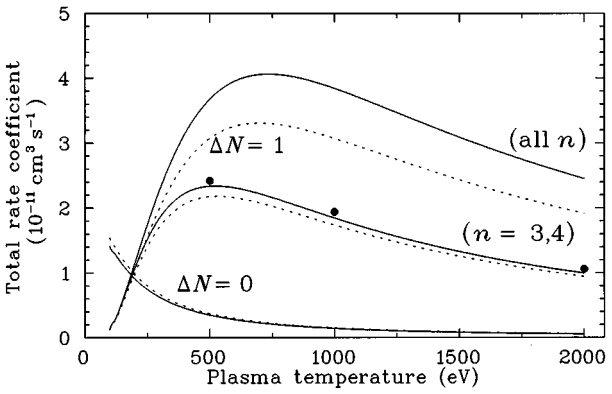

FIG. 10. Total rate coefficients for DR of Se^{25+} ions via $\Delta N=0$ and $\Delta N=1$ resonances in high-temperature plasmas as a function of the plasma electron temperature T_e. The rate coefficients were determined from the measured and the calculated DR cross sections (full and broken lines, respectively). The dots represent earlier theoretical values [14] of the total DR rate coefficients for the $\Delta N=1$ resonances with $n=3,4$. The estimated experimental errors are $\pm 15\%$ for the absolute rate-coefficient scale and $\pm 5\%$ when comparing relative contributions.

$\Delta N=1$ resonances are presented as functions of the plasma temperature T_e in Fig. 10. The contribution of the $\Delta N=0$ resonances was found from the measured cross section of Fig. 1(a), from which the RR cross section calculated by Eqs. (13) and (14) and a smooth function describing the additional nonresonant background below 50 eV (see Sec. IVB) were subtracted. The corresponding theoretical rate coefficient, derived from the calculated cross section of Fig. 1(b), is in good agreement with the experimental result. For the $\Delta N=1$ resonances we first consider the contribution of the $3l3l'$ and $3l4l'$ manifolds only. Also here the experimental and the theoretical results of the present work are in good agreement with each other; moreover, both results are close to an earlier theoretical calculation of rate coefficients [14] used in the discussion concerning the Se^{24+} soft-x-ray laser scheme (cf. Sec. I). When all $\Delta N=1$ resonances up to 1800 eV are included, the rate coefficients derived from the experimental and the theoretical results differ from each other significantly. Thus, the experiment indicates that for a temperature of $k_B T_e=1000$ eV (close to the value encountered in the x-ray laser scheme of Ref. [12]) Rydberg resonances with $n\geqslant 5$ yield $(52\pm 3)\%$ of the total DR rate coefficient, while theory predicts a relative contribution of only $\approx 42\%$ for these high-n resonances, which by their radiative decay may considerably influence the excitation of low-lying levels, including those involved in the x-ray laser scheme.

V. CONCLUSION

We have measured the energy dependence of the DR cross section due to the $\Delta N=0$ and $\Delta N=1$ resonances for fluorinelike selenium ions and compared the results with extensive calculations in the isolated-resonance approximation. The energy resolution of the measurement was $\lesssim 0.6$ eV up to 90 eV and ≈ 1.4–2 eV in the range of 90–210 eV for the $\Delta N=0$ resonances. The measured cross sections for these resonances are well reproduced by theory. In the higher energy range of 400–1800 eV, covering all $\Delta N=1$ resonances up to the $N=3$ excitation thresholds of Se^{25+}, the resolution was $\approx 4-6$ eV. The theory included configuration interaction within a manifold for low n and used a single-configuration approximation for $n\geqslant 5$. For the low-n doubly excited manifolds very good agreement between the measured and the calculated DR spectra is found, but also for the high-n doubly excited states, leading to a large energy-integrated DR cross section, the calculation reproduces the observed resonant structures rather well. On the other hand, recombinations via weaker unresolved resonances underestimated by theory appear to result in a significant additional contribution to the integrated cross section and to the total DR rate coefficient in a high-temperature plasma.

ACKNOWLEDGMENTS

We thank the TSR group, in particular M. Grieser, for the efficient support during the beam time. The experimental work has been funded in part by the German Federal Minister for Education, Science, Research and Technology (BMBF) under Contract No. 06 HD 562 I (3). The theoretical work was supported by a grant from the Office of Fusion Energy of the U.S. Department of Energy under Contract No. DE-FG05 86ER53217 with Auburn University.

[1] A. Burgess, Astrophys. J. **139**, 776 (1964).
[2] B. W. Shore, Astrophys. J. **158**, 1205 (1969).
[3] *Recombination of Atomic Ions*, edited by W. G. Graham, W. Fritsch, Y. Hahn, and J. A. Tanis, Vol. 296 of *NATO Advanced Study Institute, Series B: Physics* (Plenum, New York, 1992).
[4] L. H. Andersen, P. Hvelplund, H. Knudsen, and P. Kvistgaard, Phys. Rev. Lett. **62**, 2656 (1989).
[5] G. Kilgus, J. Berger, M. Grieser, D. Habs, B. Hochadel, E. Jaeschke, D. Krämer, R. Neumann, G. Neureither, W. Ott, D. Schwalm, M. Steck, R. Stokstad, E. Szmola, A. Wolf, R. Schuch, A. Müller, and M. Wagner, Phys. Rev. Lett. **64**, 737 (1990).
[6] G. Kilgus, D. Habs, D. Schwalm, A. Wolf, N. R. Badnell, and A. Müller, Phys. Rev. A **46**, 5730 (1992).
[7] G. Kilgus, D. Habs, D. Schwalm, A. Wolf, R. Schuch, and N. R. Badnell, Phys. Rev. A **47**, 4859 (1993).
[8] D. R. DeWitt, R. Schuch, T. Quinteros, H. Gao, W. Zong, H. Danared, M. Pajek, and N. R. Badnell, Phys. Rev. A **50**, 1257 (1994).
[9] For a review see D. A. Knapp, in Ref. [3], p. 181.
[10] M. S. Pindzola, N. R. Badnell, and D. C. Griffin, in Ref. [3], p. 93.
[11] N. R. Badnell and M. S. Pindzola, Phys. Rev. A **39**, 6165 (1989).
[12] D. L. Matthews, P. L. Hagelstein, M. D. Rosen, M. J. Eckart,

N. M. Ceglio, A. U. Hazi, H. Medecki, B. J. MacGowan, J. E. Trebes, B. L. Whitten, E. M. Campbell, C. W. Hatcher, A. M. Hawryluk, R. L. Kauffman, L. D. Pleasance, G. Rambach, J. H. Scofield, G. Stone, and T. A. Weaver, Phys. Rev. Lett. **54**, 110 (1985).

[13] M. D. Rosen, P. L. Hagelstein, D. L. Matthews, E. M. Campbell, A. U. Hazi, B. L. Whitten, B. MacGowan, R. E. Turner, R. W. Lee, G. Charatis, Gae. E. Busch, C. L. Shepard, and P. D. Rockett, Phys. Rev. Lett. **54**, 106 (1985).

[14] B. L. Whitten, A. U. Hazi, M. H. Chen, and P. L. Hagelstein, Phys. Rev. A **33**, 2171 (1986).

[15] D. R. DeWitt, D. Schneider, M. H. Chen, M. B. Schneider, D. Church, G. Weinberg, and M. Sakurai, Phys. Rev. A **47**, 1597 (1993).

[16] A. Lampert, D. Habs, G. Kilgus, D. Schwalm, A. Wolf, N. R. Badnell, and M. S. Pindzola, in *Proceedings of the VIth International Conference on the Physics of Highly Charged Ions, Manhattan, Kansas, 1992*, edited by P. Richard, M. Stöckli, C. L. Cocke, and C. D. Lin, AIP Conf. Proc. No. 274 (American Institute of Physics, New York, 1993), p. 537.

[17] E. Jaeschke, D. Krämer, W. Arnold, G. Bisoffi, M. Blum, A. Friedrich, C. Geyer, M. Grieser, D. Habs, H.-W. Heyng, B. Holzer, R. Ihde, M. Jung, K. Matl, R. Neumann, A. Noda, W. Ott, B. Povh, R. Repnow, F. Schmitt, M. Steck, and E. Steffens, in *Proceedings of the European Particle Accelerator Conference, Rome, 1988*, edited by S. Tazzari (World Scientific, Singapore, 1989), p. 365.

[18] M. Grieser, M. Blum, D. Habs, R. v. Hahn, B. Hochadel, E. Jaeschke, C. M. Kleffner, M. Stampfer, M. Steck, and A. Noda in *Cooler Rings and Their Applications*, edited by T. Katayama and A. Noda (World Scientific, Singapore, 1991), p. 190.

[19] H. Poth, Phys. Rep. **196**, 135 (1990).

[20] N. R. Badnell, J. Phys. B **19**, 3827 (1986); N. R. Badnell and M. S. Pindzola, Phys. Rev. A **39**, 1685 (1989).

[21] R. D. Cowan, *The Theory of Atomic Structure and Spectra* (University of California Press, Berkeley, 1981).

[22] R. L. Kelly, J. Phys. Chem. Ref. Data **16**, Suppl. 1, 1332 (1987).

[23] H. A. Kramers, Philos. Mag. **46**, 836 (1923).

[24] H. A. Bethe and E. E. Salpeter, *Quantum Mechanics of One- and Two Electron Atoms* (Plenum, New York, 1977), p. 322.

[25] L. H. Andersen and J. Bolko, Phys. Rev. A **42**, 1184 (1990); L. H. Andersen, G.-Y. Pan, and H. T. Schmidt, J. Phys. B **25**, 277 (1992).

[26] A. Wolf, J. Berger, M. Bock, D. Habs, B. Hochadel, G. Kilgus, G. Neureither, U. Schramm, D. Schwalm, and E. Szmola, Z. Phys. D **21**, S 69 (1991).

[27] A. Frank, A. Müller, J. Haselbauer, S. Schennach, W. Spies, O. Uwira, M. Wagner, R. Becker, M. Kleinod, E. Jennewein, N. Angert, and P. H. Mokler, Ref. [16], p. 532.

[28] A. Wolf, D. Habs, A. Lampert, R. Neumann, U. Schramm, T. Schüßler, and D. Schwalm, in *Atomic Physics 13*, edited by H. Walther, T. W. Hänsch, and B. Neitzert, AIP Conf. Proc. No. 274 (American Institute of Physics, New York, 1993), p. 228.

[29] See, e.g., J. Hahn and P. Krstic, J. Phys. B **27**, L509 (1994).

[30] O. Uwira, A. Müller, W. Spies, J. Linkemann, A. Frank, T. Cramer, L Empacher, R. Becker, M. Kleinod, P. H. Mokler, J. Kenntner, A. Wolf, U. Schramm, D. Schwalm, and D. Habs, Hyperfine Interact. (to be published).